JACS
JOURNAL OF THE AMERICAN CHEMICAL SOCIETY
ARTICLE
pubs.acs.org/JACS

Extent of M_2 δ to Ligand π-Conjugation in Neutral and Mixed Valence States of Bis(4-isonicotinate)-bis(2,4,6-triisopropylbenzoate) Dimetal Complexes (MM), Where M = Mo or W, and Their Adducts with Tris(pentafluorophenyl)boron

Philip Bunting, Malcolm H. Chisholm,* Judith C. Gallucci, and Benjamin J. Lear

Department of Chemistry, The Ohio State University, 100 West 18th Avenue, Columbus, Ohio 43210, United States

Supporting Information

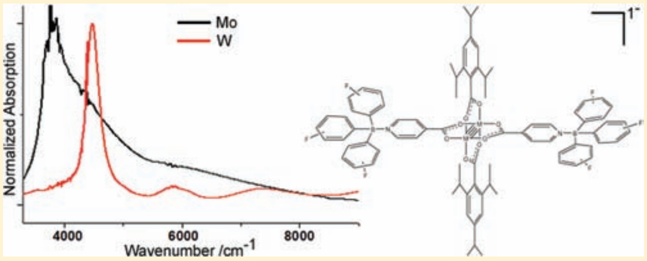

ABSTRACT: The reaction between $W_2(T^iPB)_4$, where T^iPB = 2,4,6-triisopropylbenzoate, and 2 equiv of 4-isonicotinic acid (nicH) yields the compound $W_2(T^iPB)_2(nic)_2$, **2**, and T^iPBH. Compound **2** is related to the previously reported molybdenum analog, $Mo_2(T^iPB)_2(nic)_2$, **1**. Compounds **1** and **2** react with 2 equiv of $B(C_6F_5)_3$ in THF to form the adducts $M_2(T^iPB)_2(nic\text{-}B(C_6F_5)_3)_2$, **1B** (M = Mo) and **2B** (M = W), which have been crystallographically characterized as solvates $M_2(T^iPB)_2(nic\text{-}B(C_6F_5)_3)_2 \cdot 2THF$ *n*-hexane. Compounds **1** and **2** are intensely colored due to M_2 δ to π^* MLCT transitions, and upon complexation with $B(C_5F_5)_3$ to give **1B** and **2B**, these bands shift to lower energy and gain in intensity. Each compound shows two one-electron ligand-based reductions with a $\Delta E_{1/2}$ = 120 (**1**), 300 (**1B**), 440 (**2**), and 650 mV (**2B**). The larger $\Delta E_{1/2}$ values for the tungsten compounds reflect the greater orbital mixing of the metal 5d-based M_2 δ and the nic π^* LUMO. Reduction of solutions of **1B** and **2B** with $(C_5Me_5)_2Co$ leads to the anions **1B**$^-$ and **2B**$^-$, which have been characterized spectroscopically by electron paramagnetic resonance (EPR) and UV−vis−NIR absorption. The EPR spectra of **1B**$^-$ and **2B**$^-$ are consistent with ligand-based (i.e., organic) radicals. The electronic spectra contain low-energy narrow charge resonance (IVCT) bands at 3800 (**1B**$^-$) and 4500 cm^{-1} (**2B**$^-$), consistent with fully delocalized mixed valence radical anions. The results are compared with electronic structure calculations and with the spectral features of the metal-centered delocalized mixed valence radical cations $[(Bu^tCO_2)_3M_2]_2$-μ_2-$(O_2C{-}CO_2)^+$, to which they are remarkably similar, as well as with other organic-based mixed valence systems.

INTRODUCTION

Simple mixed valence (MV) ions are composed of two redox active centers separated by a bridge where the overall charge of the ion is an odd number. In the most elementary form, these ions may be represented as $[R{-}B{-}R]^+$ or $[R{-}B{-}R]^-$ where R is the redox active center and B is the bridge. R may be a metal center, of which the so-called Creutz−Taube ion,[1] $[(H_3N)_5Ru$−μ-pyrazine−$Ru(NH_3)_5]^{5+}$, is probably the most famous example, or an organic group such as a tertiary amine[2] or nitro group,[3] which afford organic mixed valence ions upon oxidation and reduction, respectively. The commonly employed three class scheme, proposed by Robin and Day,[4] for the classification of mixed valence ions applies equally well to inorganic and organic MV ions. In this scheme, class I corresponds to a valence trapped ion where the charge is localized on one redox center, while class III corresponds to a fully delocalized ion. The intermediate class II corresponds to electronically coupled redox centers that are localized on a short time scale. Various models have been forwarded to interpret selected properties of the MV ions and particular attention has been focused on their electronic spectral features in the NIR region.[5] Class II ions show low-energy electronic transitions that may be termed intervalence charge transfer (IVCT) transitions. The energy of these transitions is solvent-dependent, consistent with their change in dipole moment as charge is transferred from one redox center to the other. For a class III compound (fully delocalized), there is no solvent dependence of this electronic transition. It is better termed a "charge resonance band",[6] since charge is not transferred between the redox active centers. As one transitions from class II to class III, the energy and shape of this electronic transition changes, and this behavior can be well accounted by the two-state model of Hush and Marcus.[7−9] As shown in Figure 1, for weakly coupled class II, there is a broad Gaussian-shaped band, which, at the class II−III border, becomes notably asymmetric with a sharp onset at low energy and with broad vibronic progressions to higher energy. As coupling increases within the class III region, the band becomes narrower and takes on a more symmetric shape. For class III systems, the energy of the band, *E*, is related to the magnitude of the electronic coupling of the two states, $\mathbf{H_{AB}}$, by the simple relationship $E = 2\mathbf{H_{AB}}$. This has all been addressed in detail in a past review.[10]

Received: November 3, 2010
Published: March 24, 2011

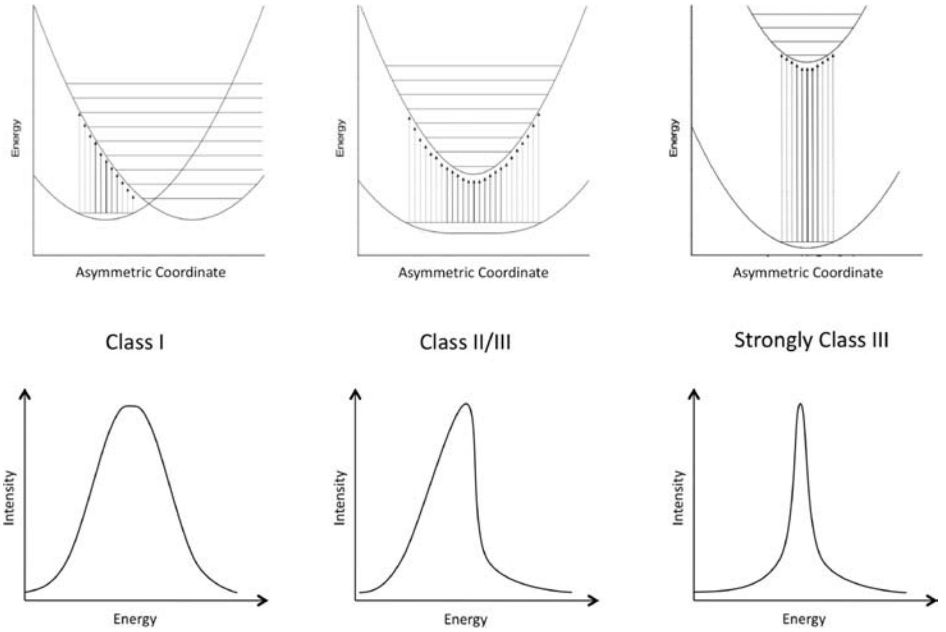

Figure 1. Schematic diagram showing how the shape of the IVCT band for symmetric systems under the two-state model changes as a function of coupling. (top) Potential energy surfaces with vibrational levels shown and (bottom) the associated band shapes. The dashed band shape is that shown for class I systems.

Scheme 1. Examples of Organic Mixed Valence Ions[a]

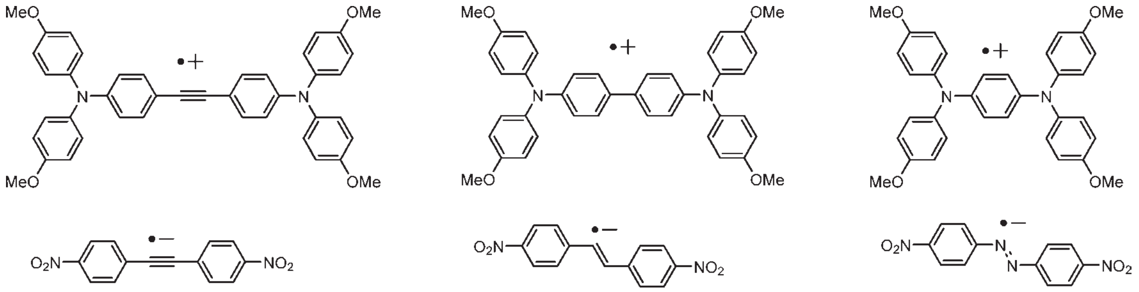

[a] The triarylamine-based ions are from ref 2 and the nitro-based ions are from ref 3.

The two-state model as advanced by Marcus is an excellent model in predicting the rates of electron transfer for outer-sphere processes, especially where the two redox-active centers are not identical. This model explains the rate acceleration with increasing driving force, $\Delta G°$, and the retardation of rate that occurs when $\Delta G°$ becomes too negative, the so-called inverted region. The two-state model is, however, not appropriate for a detailed understanding of the properties of MV ions of the form $[R{-}B{-}R]^{\pm}$ where the two redox centers are equivalent and the bridge is a functional group that electronically couples them. Here, at minimum, a three-state model must be invoked. In a molecular orbital picture, the orbitals of the redox center mix with those of the bridge.[11] Typically, the *connectivity* of R−B−R unit involves σ orbitals, and the electronic *coupling* in the MV ion involves the π-orbitals. This is readily apparent from the organic radical cations and anions shown in Scheme 1 and is similarly seen in the Creutz−Taube ion where Ru d orbitals interact with the π-orbitals of the pyrazine bridge.

In our laboratory, we have been examining the electronic coupling of two quadruply bonded dinuclear centers linked by dicarboxylate bridges that have extended π-systems: $[MM]{-}[O_2C{-}B{-}CO_2]{-}[MM]$ where $[MM] = Mo_2$, MoW, or W_2 supported by three ancillary carboxylate ligands.[12] Here the MM δ orbitals interact with the π-system of the bridge, leading to the schematic MO diagram shown in Figure 2. Based on energetic considerations when the bridge B is tethered by carboxylate groups, it is the LUMO of the bridge (π^*) that interacts most strongly with the MM δ orbitals. For a class III MV ion, we have observed the solvent-independent "IVCT" or charge resonance band. In addition, we have noted that the MLCT is also affected by electronic coupling, losing both its solvent dependence and breadth as the electronic coupling moves the potential energy surfaces associated with the ground and excited states toward one another along the symmetric coordinate.[13] In this regard, we have emphasized the importance of examining the MLCT bands in addition to the IVCT bands in both their MV and neutral (nonmixed valence) states.

While the bridge serves to couple the redox-active centers in $[M_2]{-}O_2C{-}B{-}CO_2{-}[M_2]$ complexes, it is also apparent that for $L{-}[M_2]{-}L$ systems, where L = a conjugated π-system, the M_2 δ orbital should couple the ligands L such that $[L{-}[M_2]{-}L]^-$ could be considered either as a ligand-based mixed valence anion or as a metal-stabilized organic radical anion. Again, we can refer to a simple orbital picture based on the M_2 δ

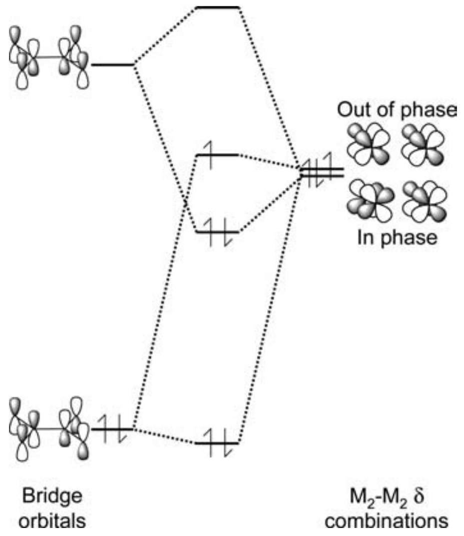

Figure 2. Schematic molecular orbital diagram for M_2-B-M_2 complexes in their $+1$ mixed valence state, where B = oxalate.

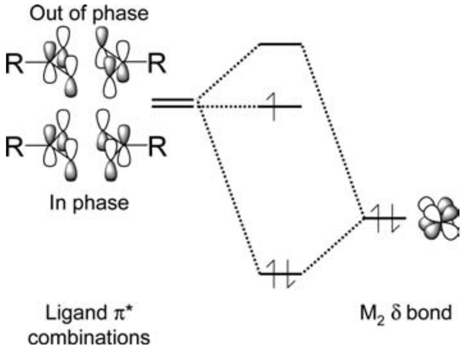

Figure 3. Schematic molecular orbital diagram for $L-M_2-L$ complexes in their -1 mixed valence state.

orbital interacting with combinations of the ligand π-system, leading to the orbital interaction diagram shown in Figure 3. Here a MV radical anion $[L-[M_2]-L]^-$ would be expected to possess a low-energy LUMO → LUMO + 1 charge resonance (IVCT) band and a higher energy MLCT band. Just as in the M_2-B-M_2 case, the properties of these transitions should provide insight into the nature of the MV ion. In earlier work in this laboratory, we had seen evidence for such ligand-based mixed valency in the chemistry of *trans* $M_2(T^iPB)_2L_2$ compounds where M = Mo or W and L = an azulene carboxylate[14−16] or thienyl carboxylate.[17] However, as with many organic radical ions, these were kinetically labile. We reasoned that if, somehow, we might sterically and electronically protect these ligand-based radical ions we might further study the influence of M_2 δ-ligand π-conjugation. Herein, we describe our results that were inspired by this line of reasoning.

■ RESULTS AND DISCUSSION

Synthesis. The reaction between $W_2(T^iPB)_4$ and 4-isonicotinic acid (2 equiv) in toluene gave $W_2(T^iPB)_2(nic)_2$, **2**, where T^iPB is 2,4,6-triisopropylbenzoate and nic = 4-isonicotinate with the liberation of T^iPBH (2 equiv). This green crystalline compound is analogous to the previously reported $Mo_2(T^iPB)_2(nic)_2$, **1**, which has a trans-disposition of ligands and exists as a coordination polymer in the solid-state due to weak N-to-M axial ligation.[18]

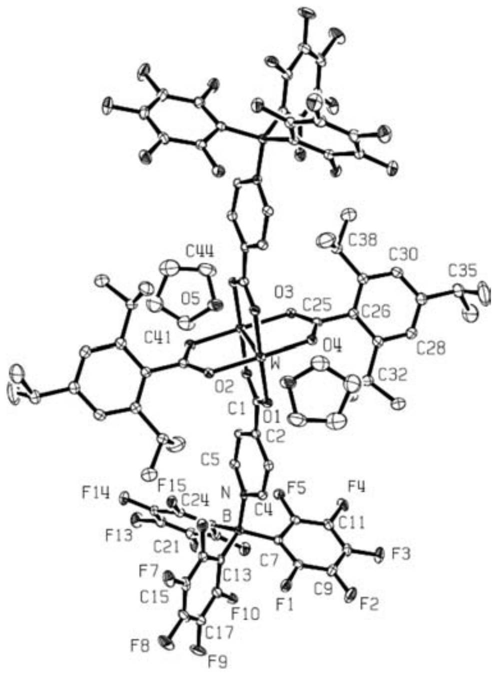

Figure 4. ORTEP drawing of **2B**. The ORTEP plot is drawn with 30% probability ellipsoids for the non-hydrogen atoms. The hydrogen atoms are omitted for clarity. The molecule contains a crystallographic inversion center, which is located in the middle of the W−W bond. The solvent molecule of *n*-hexane is also omitted from this plot.

The reactions between either **1** or **2** and $B(C_6F_5)_3$ (2 equiv) in THF proceed smoothly at room temperature to give **1B** (M = Mo) and **2B** (M = W). These reactions proceed with a distinct color change: **1** (red) → **1B** (purple) and **2** (green) → **2B** (pale blue).

Crystals of **1B** adequate for single-crystal X-ray diffraction were grown from a THF/hexane solution. Similar crystals of **2B** were grown in cold toluene. Both molecules crystallized in the $P\overline{1}$ space group, and they are isostructural. They have a crystallographically imposed center of inversion located at the midpoint of the M−M bond. The molecular structure of the tungsten compound, **2B**, is shown in Figure 4. An ORTEP drawing of the analogous structure of **1B** is included in the Supporting Information. Crystallographic data is summarized in Table 1. The central $M_2(O_2C)_4$ core is typical of MM quadruply bonded compounds supported by carboxylates.[19] The two isonicotinate ligands are mutually trans and the O_2C and C_5N planes are aligned so as to allow extended ligand $\pi-M_2$ $\delta-$ligand π interactions. The dihedral angles between the O_2C and C_5N least-squares planes are 12.8(2)° in **1B** and13.5(3)° in **2B**. A similar pattern of extended $L\pi-M_2\delta-L\pi$ interactions is seen in the structures of $M_2(T^iPB)_2(O_2C\text{-thienyl})_2$[17] compounds and in the compound $W_2(T^iPB)_2$(6-carboethoxy-2-azulene carboxylate)$_2$.[16] The slight curvature of the extended π system in these compounds is reminiscent of that seen in dinuclear polyyne bridged complexes, $[M]-(C_2)_n-[M]$.[20] Finally, the central $[M_2]$ unit has weak axial coordination of the THF molecules with long M···O distances, > 2.5 Å, in contrast to the M—O carboxylate distances, which fall in

Table 1. Crystallographic Data for 1B and 2B

compound	1B	2B
formula	$C_{80}H_{54}B_2F_{30}Mo_2N_2O_8$ + 2THF + n-hexane	$C_{80}H_{54}B_2F_{30}N_2O_8W_2$ + 2THF + n-hexane
formula wt	2185.13	2360.95
crystal color, habit	brown, rectangular block	green, rectangular block
crystal dimens (mm^3)	0.15 × 0.23 × 0.31	0.08 × 0.12 × 0.35
crystal syst	triclinic	triclinic
space group	$P\bar{1}$	$P\bar{1}$
a (Å)	10.4023(1)	10.4199(1)
b (Å)	15.7963(1)	15.8525(2)
c (Å)	16.9541(1)	16.8803(2)
α (deg)	115.641(1)	115.978(1)
β (deg)	94.922(1)	95.206(1)
γ (deg)	96.875(1)	96.271(1)
vol ($Å^3$)	2463.82(3)	2461.44(5)
Z	1	1
temp (K)	150(2)	150(2)
density (calcd) (Mg/m^3)	1.473	1.593
GOF on F2	1.048	1.077
final indices $[I > 2\sigma(I)]$	R1 = 0.032, wR2 = 0.084	R1 = 0.0261, wR2 = 0.0639

Table 2. Selected Bond Distances for 1B and 2B

	distance, Å	
bond	1B	2B
M−M	2.1153(4)	2.2158(3)
O(1)−M	2.1098(14)	2.064(2)
O(2)−M	2.0935(14)	2.048(2)
O(3)−M	2.0984(14)	2.072(2)
O(4)−M	2.0946(14)	2.074(2)
O5−M	2.564(2)	2.525(3)
N−B	1.624(3)	1.615(4)

the range of 2.05−2.10 Å. Selected bond distances for the two compounds are given in Table 2.

Electronic Structure Calculations. In order to aid in the interpretation of the spectroscopic and electrochemical data pertaining to the complexes **1**, **1B**, **2**, and **2B**, we undertook electronic structure calculations on model compounds (**1′**, **1B′**, **2′**, **2B′**), where formate is substituted for the $\mathrm{T^iPB}$ ligands. This substitution saves on computational time and is not an unreasonable approximation since the $\mathrm{T^iPB}$ rings are twisted out of conjugation with their carboxylate linkers. The gas-phase minimum energy structures were determined in C_1 symmetry and possessed the planar alignment of the two trans $O_2C{-}C_5H_4N$ units.

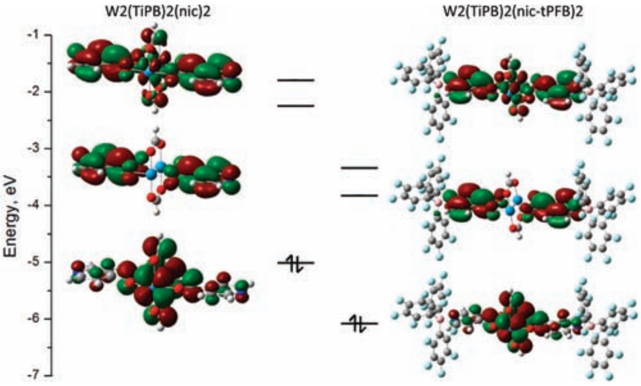

Figure 5. Energy level diagram for **2′** and **2B′** showing the HOMO, LUMO, and LUMO + 1.

Table 3. Calculated Frontier MO Energies (eV)[a]

compound	HOMO δ	δ^*	L π_1^*	L π_2^*	ΔE
1	−5.48	−2.24	−2.19	−1.86	0.33
1B	−6.46	−3.19	−3.75	−3.43	0.32
2	−5.01	−1.50	−2.25	−1.79	0.46
2B	−6.07	−2.52	−3.83	−3.35	0.48

[a] L π_1^* = in-phase combination (LUMO or LUMO + 1); L π_2^* = out-of-phase combination (LUMO + 1 or + 2); ΔE = L π_2^* − L π_1^*.

For **1′**, **1B′**, **2**, and **2B′**, the HOMO was the M_2 δ orbital with some mixing with the isonicotinate ligands. For and **1B′**, **2**, and **2B′**, the LUMO and LUMO + 1 were, respectively, the in-phase and out-of-phase combinations of the ligand π^* orbitals, as predicted by the schematic MO interaction diagram show in Figure 3. However for **1′**, these combinations were the LUMO + 1 and LUMO + 2, the LUMO being the MM δ^*. The comparison between the model compounds **1′** and **1B′**, as well as **2′** and **2B′**, reveals some striking trends. (i) Complexation to $B(C_6F_5)_3$ notably stabilizes the energy of the M_2 δ orbital (HOMO). (ii) The LUMO is also stabilized, but to a greater extent, thus reducing the HOMO−LUMO gap upon complexation with $B(C_6F_5)_3$. (iii) Complexation to $B(C_6F_5)_3$ has little effect on the energy gap between the in-phase and out-of-phase combinations of the lowest energy ligand π^* orbitals. These changes are illustrated by the comparison of the calculated frontier molecular orbital energies for compounds **2′** and **2B′**, as shown in Figure 5. The calculated energies of these frontier orbitals are given in Table 3.

We also note that as a result of the 3-fold symmetry of $B(C_6F_5)_3$, it is not well matched to electronically couple the aryl rings to the nic donor (as seen in Figure 5). For this reason,

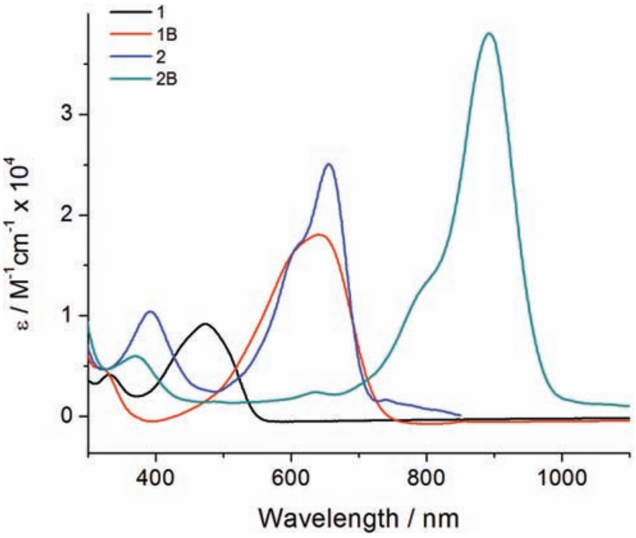

Figure 6. UV−vis spectra for **1**, **1B**, **2**, and **2B** in THF at room temperature.

Table 4. Redox Potentials (V) for the Three Redox Events Observed for 1, 1B, 2, and 2B in THF Referenced to the Fc/Fc$^+$ Couple

complex	E_1	E_2	E_3	$\Delta E_{2,3}$
1	−0.02	−2.48	−2.60	0.12
1B	0.42	−1.50	−1.80	0.30
2	−0.24	−1.88	−2.32	0.44
2B	−0.13	−1.27	−1.92	0.65

complexation of $B(C_6F_5)_3$ to **1** and **2** affects the energies of the nic π and M_2 δ orbitals, without substantially affecting their nature and thus, affects the energy, but not the nature, of the electronic transitions in these complexes.

Electronic Absorption Spectra. The room-temperature optical spectra of the four compounds **1**, **1B**, **2**, and **2B** are shown in Figure 6. The intense absorptions in the visible region arise from the M_2 δ to isonicotinate π*, ^{1}MLCT, transition. The trends in the energies associated with this transition correlate well with the expectations based on the calculated HOMO−LUMO gaps as can be seen from an inspection of Figure 3. The intensity of the MLCT transitions increases with decreasing energy, and the ε values range from 9200 M^{-1} cm^{-1} for **1** to 38000 M^{-1} cm^{-1} for **2B**. Such a trend is expected, because coupling between the ligands and the M_2 center (and, hence ε) will increase as the energy gap between them decreases.

We also comment that, in solution, there is a Boltzmann distribution of rotamers deviating from the ground-state planar D_{2h} conformation, and each of these gives rise to a slightly different MLCT transition energy. Either an increase in π* backbonding or a reduction of the temperature will favor the D_{2h} conformation, shifting the weighted distribution toward planarity. This reasoning explains the fact that the red shift of these ^{1}MLCT bands (**1** → **2B**) is accompanied by a decrease in bandwidth, consistent with enhanced M_2 δ to nic π* backbonding (as the M_2 δ−nic π* energy gap decreases). Furthermore, lowering the temperature is found to lead to a sharpening of the vibronic features, as a more planar structure in the compounds is reinforced. A comparison of the room-temperature spectra of **1B** and **2B** to those at 100 K (recorded in 2-MeTHF) is given in the Supporting Information.

We have also examined the solvent dependence of the ^{1}MLCT for compounds **1B** and **2B** in toluene, dichloromethane, and THF. These spectra are shown in the Supporting Information. For both compounds, the spectra in THF are red-shifted relative to the other solvents, which is not surprising because THF can coordinate to the M_2 center (as seen in Figure 4) and stabilize the positive charge on the M_2 core that results in the photoexcited state. The spectra for the molybdenum complex, **1B**, in CH_2Cl_2 and toluene have λ_{max} at 626 and 599 nm, respectively, while for the tungsten complex, **2B**, λ_{max} is at 850 for both CH_2Cl_2 and toluene. We propose this reflects the greater delocalization of the ligand-based negative charge in the case of the tungsten complex, **2B**. In other words, the ^{1}MLCT for **2B** has a negligible change in dipole moment, while that for **1B** has at least some change. Note that the dielectric constants for CH_2Cl_2 and toluene are 8.93 and 2.38, respectively. This significant difference makes them good solvents for evaluating the relative change in dipole moment for a MLCT transition.

Electrochemical Data. The four compounds under study have been examined by cyclic voltammetry and differential pulse voltammetry in THF solutions. The data are summarized in Table 4. All four compounds show three redox events. The most positive of these is associated with the removal of a single electron from the M_2^{4+} core. The remaining two events, which occur at much more negative potentials, are both one-electron reductions of the ligands. As expected, it was found that it is easier to oxidize the W_2^{4+} center than the Mo_2^{4+} center and that complexation with $B(C_6F_5)_3$ shifts these oxidation potentials to more positive values. Similarly, the ligand based reduction waves occur at a less negative potential in the $B(C_6F_5)_3$ adducts, relative to **1** and **2**. These results are in line with expectations based upon the calculations on the model compounds (Table 3) as well as with chemical intuition.

Of particular note is the magnitude of the splitting between the reduction waves. The splitting reflects a combination of the magnitude of the electronic coupling and electrostatic effects, which vary with solvent and counterions. However, for pairs of related ions that differ only by metal ions Mo versus W, which have effectively identical size and solvent effects, the magnitude of the separation of the two waves is informative with respect to the relative electronic coupling of the two isonicotinic ligands via the M_2δ orbital. The splitting is 0.12, 0.30, 0.44., and 0.65 mV for **1**, **1B**, **2**, and **2B**, respectively. Notably, the magnitude of this coupling is always bigger for the tungsten complexes due to the greater W_2 δ−ligand π* interaction. Upon adduct formation with $B(C_6F_5)_3$ there is a further increase in separation, which is due to the stabilization of the negative charge on the ligands by the $B(C_6F_5)_3$. This also has the effect of increasing the coupling (relative to **1** and **2**) of the ligand-based states with the lower energy M_2-based state.

Inspection of the reduction waves for the tungsten complex **2B** reveals the presence of an additional species with a reduction potential slightly more negative than the first event. The sample under investigation was taken from the crystals that were subject to elemental analysis, so we are not inclined to the view that the sample was impure. Rather, we propose that under the dilute condition of **2B** in the donor solvent THF some equilibrium exists where one $B(C_6F_5)_3$ unit dissociates from a nic ligand. Some support for this is seen in the electrochemical behavior of **2B** in dichloromethane, where this extra reduction is not observed. In CH_2Cl_2, the second reduction is found to be irreversible. A similar feature is seen in the electrochemistry of **1B** in THF. However, **1B** is not soluble in CH_2Cl_2, and we assume that this has similar origins. Cyclic voltammograms for **1B** and **2B** showing the oxidation and reduction waves are given in the Supporting Information.

Mixed Valence Anions: $1B^-$ and $2B^-$. Reduction of **1B** and **2B** with $Cp_2{}^*Co$ in THF gave reduced ions $\mathbf{1B}^-$ and $\mathbf{2B}^-$ whose spectral features are shown in Figure 7. Upon reduction of **1B** to $\mathbf{1B}^-$, the color of the solution changed from blue to green. There was a very slight change of color upon reduction of **2B** to $\mathbf{2B}^-$, mainly changing the shade of blue-green. Of prime significance is the appearance of new sharp electronic bands in the NIR region, namely at 3800 cm^{-1} for $\mathbf{1B}^-$ and 4500 cm^{-1} for $\mathbf{2B}^-$. These bands are sharp, with the width at half height for $\mathbf{2B}^-$ being only 300 cm^{-1}. In addition, we note that the band for $\mathbf{1B}^-$ is noticeably more asymmetric than that for $\mathbf{2B}^-$. We assign these bands to the charge resonance transitions of fully delocalized mixed valence ligands. In a simple MO description (Figure 3), they correspond to the promotion of the single electron from the LUMO to the LUMO + 1. This is consistent with the similarity of the EPR spectra of $\mathbf{1B}^-$ and $\mathbf{2B}^-$ (discussed below).

In addition to the electronic transition in the NIR, each compound also shows a strong absorption in the visible region corresponding to the ^{2}MLCT. In orbital terms, this is promotion of a single electron from the M_2 δ orbital to the SOMO. The ^{2}MLCT band for $\mathbf{1B}^-$ is lower in energy than that for **1B** and that for $\mathbf{2B}^-$ is higher in energy than that for **2B**. Also, the ^{2}MLCT bands are narrower than their singlet counterparts (see Supporting Information). Finally, based on the shape of these electronic NIR transitions, we assign $\mathbf{1B}^-$ as near the Robin−Day class II/III border and $\mathbf{2B}^-$ well within class III.

EPR Spectrum of $1B^-$ and $2B^-$. Reduction of **2B** with $Cp_2{}^*Co$ in THF leads to an EPR-active species, $\mathbf{2B}^-$, that has a single resonance at $g \approx 2.04$ (see Supporting Information). This shows no hyperfine coupling to ^{183}W and, in contrast to tungsten-based W_2 δ^1 electrons with $g \approx 1.8$, is close to the free electron value. This is consistent with a ligand-centered radical anion. Reduction of **1B** with $Cp_2{}^*Co$ similarly leads to an EPR-active species with a single resonance at $g \approx 2.01$ (see Supporting Information), consistent with a ligand-centered radical anion. This signal showed no hyperfine coupling to ^{95}Mo or ^{97}Mo.

Comparisons with Related Mixed Valence Ions. *Oxalate Bridged M_2 Containing Complexes.* We are struck by the remarkable relationship between the spectra and electrochemical data for the MV ions that result for the oxalate-bridged species of the form $[(Bu^tCO_2)_3M_2]_2$-μ_2-$(O_2C{-}CO_2)^+$ and the anions $\mathbf{1B}^-$ and $\mathbf{2B}^-$. As is evident from Figures 2 and 3, the radical cations are metal-centered and the anions are ligand-centered. For the former, the splitting of the M_2 δ orbitals in the neutral complexes is a measure of the electronic coupling of the two M_2 centers. For molybdenum, this is ∼0.3 eV, while for tungsten, this is ∼0.5 eV. For **1B′** and **2B′**, the energy of the separation of the in-phase and out-of-phase ligand π^* orbitals (0.32 and 0.48 eV, respectively) is also a measure of the coupling of the ligand π systems in the neutral complexes. Upon oxidation of the former and reduction of the latter, the coupling will increase in the resultant MV ions, as we have previously discussed,[13] because the MO picture does not accurately reflect the nature of coupling between electronic *states*. Nevertheless, the fact that the calculated energy separation between the in-phase and out-of-phase ligand π^* orbitals in the anions ($\mathbf{1B}^-$ and $\mathbf{2B}^-$) is virtually identical to the separation of the two M_2 δ combinations in the oxalate-bridged cations seems more than fortuitous.

This similarity of calculated energy splitting is remarkably born out in the observed electrochemical and spectroscopic features of the related cations and anions, as can be seen from an inspection of Table 5. As $\Delta E_{1/2}$ increases so does the ν_{max} of the charge resonance band, which is consistent with class III behavior. The shape of the charge resonance bands also tracks with $\mathbf{H_{AB}}$, and as $\mathbf{H_{AB}}$ increases, the bands get sharper and more symmetric. For a comparison, we show the IVCT bands of the oxalate bridged cations in Figure 8. Perhaps the only major difference in comparing the radical cations and the anions is in the bandwidths of these charge resonance transitions. The MV anions are notably sharper, and the $\Delta\nu_{1/2}$ of 300 cm^{-1} for $\mathbf{2B}^-$ is truly remarkable. Although we have not yet obtained the anions

Table 5. Comparison of Select Parameters for Ligand- and Metal-Based Mixed Valence Complexes

complex	$\Delta_{1/2}$, mV	$K_c{}^a$	ν_{max},^{b} cm^{-1}	$\Delta\nu_{1/2}$,^{b} cm^{-1}	$\mathbf{H_{AB}}$,^{c} cm^{-1}
$\mathbf{1B}^-$	300	1.22×10^5	3800	1000	1900
$\mathbf{2B}^-$	650	1.04×10^{11}	4500	300	2250
$Mo_4oxalate^+$	280	5.57×10^4	4000	2800	2000
$W_4oxalate^+$	717	1.42×10^{12}	5960	940	2980

[a] $K_c = \exp(\Delta E_{1/2}/25.69)$ at 298 K. [b] For the IVCT bands. [c] Assuming the class III limit, where $\mathbf{H_{AB}} = \nu_{max}(cm^{-1})/2$.

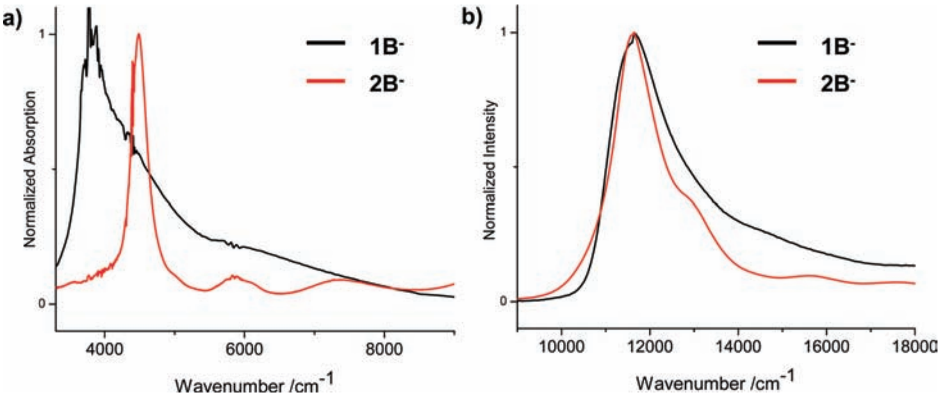

Figure 7. Comparison of the (a) IVCT and (b) MLCT bands of $\mathbf{1B}^-$ and $\mathbf{2B}^-$ in THF at room temperature. All of the bands are presented normalized, for ease of comparison.

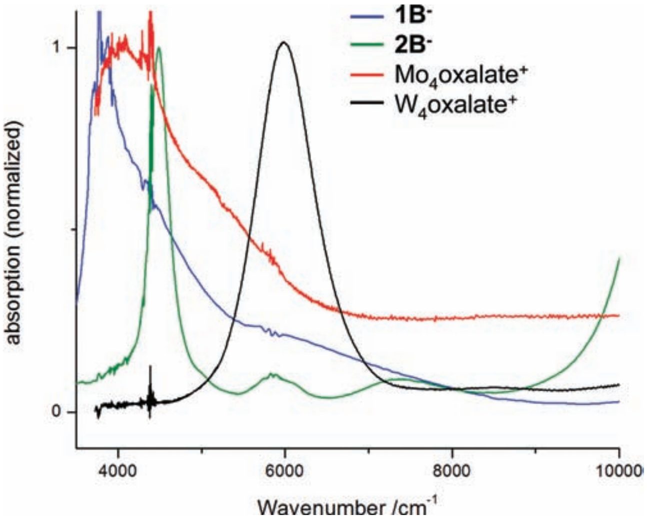

Figure 8. Comparison of the IVCT bands for the mixed valence anions $\mathbf{1B}^-$ (blue) and $\mathbf{2B}^-$ (green) with the IVCT bands for the mixed valence cations Mo_4oxalate$^+$ (red) and W_4oxalate$^+$ (black). All spectra were taken in THF.

$\mathbf{1B}^-$ and $\mathbf{2B}^-$ as pure crystalline salts, we can reasonably estimate the intensity of the charge resonance bands in the NIR to be ~ 10000 M^{-1} cm^{-1}.

Hupp's Compounds. The similar relationships noted above between the cations $[M_2{-}B{-}M_2]^+$ and the anions $[L{-}M_2{-}L]^-$ may, in part, be related to the distance between the two redox-active centers. For the oxalate-bridged system, the M_2 centers are 6 Å apart, while in **1B** and **2B**, the *ipso*-carbons of the nic ring are similarly separated by the $M_2{-}(O_2C)_2$ unit at a distance of 8 Å. Hupp and co-workers have previously examined the redox properties of molecular rectangles of the type represented schematically by **A** below.[21−23]

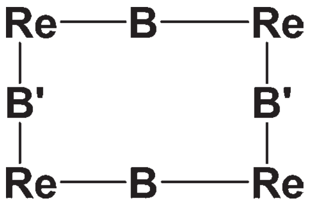

In **A**, B′ is a short bridge such as 2,2′-bisbenz-imidazolate, and B was varied to include extended bridging π-systems, such as 4,4′-bipyridine and even porphyrins. In this architecture, the two π systems of the larger bridge B were brought into close proximity, ~6 Å, due to the shorter bridge, B′. Upon reduction, these formed MV ions, which showed NIR transitions, which were assigned as IVCT. These are notably higher in energy than those for $\mathbf{1B}^-$ and $\mathbf{2B}^-$ and are also notably broader. The authors claimed that these were class II on the Robin−Day scheme and the primary mechanism of coupling was through the direct, but weak, $\pi{-}\pi$ interactions of B with B and not via a direct coupling involving the rhenium $t_{2g}{}^6$ centers. The spectroscopic features described herein for $\mathbf{1B}^-$ and $\mathbf{2B}^-$ certainly would support this.

Organic Mixed Valence Anions. It is also interesting to compare the spectroscopic features of the organic radical anions studied by Nelsen and co-workers.[3,24,25] Typically, the nitro derivatives of the type shown in Scheme 1 display intense NIR absorptions, which can be classified as belonging to class III or class II depending both upon the nature of the bridge (C≡C, C=C, N=N) and the solvent where the countercation is Na^+. Here solvents, such as THF, that solvate Na^+ well can lead to class III behavior, whereas CH_3CN leads to class II spectra, presumably because of higher ion pairing (charge pinning) with the anion. Similar spectral features have been observed by Lambert for mixed valence radical cations of diamines. Notably, in these organic MV ions as one progresses from class II toward class III the bands become more asymmetric. However, even the phenylene-bridged diamine radical cation is considered as class II, valence trapped, and has a larger $\Delta\nu_{1/2}$ than the MV ions $\mathbf{1B}^-$ and $\mathbf{2B}^-$.

CONCLUDING REMARKS

A comparison of the spectroscopic and electrochemical data for the compounds **1** and **2**, their $B(C_6F_5)_3$ adducts **1B** and **2B**, and their radical anions $\mathbf{1B}^-$ and $\mathbf{2B}^-$ reveals a fascinating trend in M_2 δ to ligand π conjugation. The similarity of the electronic coupling of the ligands in the radical anions with the electronic coupling of the M_2 centers in the oxalate-bridged compounds is truly notable. We propose that this similarity arises for two principal reasons. (1) The distances between the two redox centers, the two M_2 centers in the oxalate-bridge cations, and the isonicotinic ligands are similar. (2) In both cases, the coupling arises via M_2 $\delta{-}CO_2$ π^* orbital interactions, and the energy separation between the M_2 δ HOMO and the bridge/ligand LUMO is of comparable energy. Finally, in comparing our data with earlier studies of organic MV ions, we note that the M_2 δ unit is more effective in achieving delocalization (class III properties) than the C≡C, C=C, N=N, or C_6H_4 bridges employed in the compounds displayed in Scheme 1. Further studies aimed at isolating the salts of $\mathbf{1B}^-$ and $\mathbf{2B}^-$ in a pure form and other related M_2 δ mediated ligand MV anions are underway.

EXPERIMENTAL SECTION

General Procedures. All reactions were carried out under dry and inert atmosphere (N_2 or argon) using standard Schlenk and glovebox techniques. All solvents were dried and degassed by standard methods and distilled prior to use. Ditungsten and dimolybdenum tetratriisopropylbenzoate ($Mo_2T^iPB_4$ and $W_2T^iPB_4$, respectively) were prepared by the literature procedure.[15,26] Isonicotinic acid (Hnic) and $B(C_6F_5)_3$, were purchased from commercial sources and used as received. Decamethylcobaltocene was purchased from commercial sources and sublimed prior to use. Preparation of **1** has previously been reported.[18]

Instrumentation. UV−vis and NIR spectra were collected on a Perkin-Elmer Lambda 900 UV−vis−NIR spectrometer. Low-temperature UV−vis spectra were acquired on the same UV−vis spectrophotometer using a Specac variable-temperature cryostat that employs a permanently sealed liquid IR cell with CaF_2 windows. EPR spectra were acquired at room temperature on a Bruker ESP300 in 2-MeTHF or THF.

Preparation of $W_2(T^iPB)_2(nic)_2\cdot THF$ (2). A Schlenk flask was charged with 1 equiv of W_2(triisopropylbenzoate)$_4$ and 2 equiv of isonicotinic acid. On a Schlenk line, enough acetonitrile was added to the flask to fully dissolve the $W_2(T^iPB)_4$, though the isonicotinic acid was not completely soluble. The resulting solution was stirred for 3 days, at which time no solid isonicotinic acid remained in the flask. During the course of the reaction, the solution had changed from bright red to green, and a green precipitate was formed. The solid was collected by centrifugation and washed three times with hexanes and then dried under vacuum. Yield (40%).

Anal. Calcd for $W_2C_{44}H_{54}N_2O_8$: C, 48.91; H, 5.30; N, 2.38. Found: C, 48.63; H, 5.07; N, 2.20. ^{1}H NMR (250 MHz, THF-d_8): δ 1.0 (d, 12H), 1.2 (d, 6H), 2.8 (m, 3H), 7.0, (s, 2H), 7.9, (d, 2H), 8.8, (d, 2H).

Preparation of $Mo_2(T^iPB)_2(nic\text{-}B(C_6F_5)_3)_2$, (1B). A Schlenk flask was charged with 1 equiv of **1** and 2 equiv of $B(C_6F_5)_3$ in a glovebox. On a Schlenk line, enough THF was added to dissolve **1**. The reaction was left to stir for two days during which time the solution changed color from green to blue. After this, the THF was removed under vacuum to a minimal volume. To this, hexanes were added in order to crash out the desired product, which was collected via centrifugation and washed three times with hexanes. The product was then dried, and the solid was collected. Yield (65%).

Anal. Calcd for $Mo_2C_{80}H_{54}B_2F_{30}N_2O_8$: C, 49.15; H, 2.79; N, 1.43. Found: C, 48.93; H, 2.85; N, 1.39. ^{1}H NMR (250 MHz, THF-d_8): δ 1.0 (d, 12H), 1.3 (d, 6H), 2.9 (m, 3H), 7.1, (s, 2H), 8.5, (d, 2H), 9.1, (d, 2H).

Preparation of $W_2(T^iPB)_2(nic\text{-}B(C_6F_5)_3)_2\cdot THF$ (2B). Compound **2B** was made in a similar manner as **1B**. Alternatively, **2B** was made by charging one flask with 1 equiv $W_2(T^iPB)_4$ and a second flask with 2 equiv of isonicotinic acid and 2 equiv of $B(C_6F_5)_3$ in a glovebox. To the second, toluene was added on a Schlenk line, and the solution stirred until the isonicotinic acid was completely dissolved. This solution was then transferred to the first flask. Upon the addition of the solution, the color of the reaction changed from bright red to emerald green and, finally, to blue. The reaction was stirred for 3 days and then placed in a refrigerator at 10 °C for 2 weeks after which time crystals appropriate for single-crystal X-ray diffraction were found to have grown in the flask. A few crystals were removed for X-ray diffraction, the rest were washed three times with hexanes and dried in vacuum. Yield (34%).

Anal. Calcd for $W_2C_{84}H_{62}B_2N_2O_9$: C, 46.46; H, 3.10; B, 0.95; N, 1.23. Found: C, 46.10; H, 3.37; B, 0.52; N, 1.36. ^{1}H NMR (250 MHz, THF-d_8): δ 1.0 (d, 12H), 1.2 (d, 6H), 2.8 (m, 3H), 7.0, (s, 2H), 8.2, (d, 2H), 9.0, (d, 2H).

Preparation of the Anions $1B^-$ and $2B^-$. The reactions between solutions of **1B** or **2B** and $Cp_2{}^*Co$ in either THF or 2-MeTHF were carried out in a 1:1 ratio yielding an immediate color change. These freshly prepared solutions were then examined by EPR and UV−vis−NIR spectroscopy. The NIR bands are shown in Figure 8, and the MLCT bands of the anions are shown in Figure 7. EPR spectra are given in Figure S4, Supporting Information. The following represents an initial attempt to isolate a salt in a pure microcrystalline form.

$Mo_2(T^iPB)_2(nic\text{-}B(C_6F_5)_3)_2$, **1B** (31.7 mg, 0.0162 mmol), and $CoCp_2{}^*$ (5.5 mg, 0.017 mmol) were put in separate Schlenk flasks. Compound **1B** was dissolved in minimal THF and cooled in an ice bath, while the $CoCp_2{}^*$ was dissolved in excess hexanes. The $CoCp_2{}^*$ solution was transferred to the solution of **1B**, causing an immediate color change from blue to green and a green precipitate to fall out of solution. The mixture was stirred for 2 min, and then the green precipitate was collected via filtration, washed three times with hexanes, and dried under vacuum. Yield (29.8 mg, 0.0130 mmol, 80%).

Anal. Calcd for $Mo_2C_{100}H_{84}B_2F_{30}N_2O_8Co$: C, 52.58; H, 3.71; N, 1.23. Found C, 49.00; H, 4.08; N, 0.97.

DFT Calculations. Molecular and electronic structure determination were performed under C_1 symmetry using the Gaussian 98 program[27] employing the B3LYP functional[29−31] in conjugation with the 6-31G* basis set[28] for H, C, O, N, and B and the SDD energy-consistent pseudopotential basis set[32] for Mo and W. All geometries were fully optimized at the above levels using the default optimization criteria of the program. Orbital analyses were completed with GaussView.[33]

Crystallographic Section. The data collection crystal was a dark brown rectangular block for **1B** and a green rectangular block with a wedge-shaped cross-section for **2B**. Both data sets were measured at 150 K using an Oxford Cryosystems Cryostream Cooler and a Nonius Kappa CCD diffractometer with Mo Kα radiation. Further experimental details, as well as the structures of **1B** and **2B** can be found in the Supporting Information.

■ ASSOCIATED CONTENT

Ⓢ Supporting Information. Electronic absorption spectra for **1B** and **2B** in various solvents and at 100 K in 2MeTHF, MLCT bands for the anions $\mathbf{1B}^-$ and $\mathbf{2B}^-$, EPR spectra for $\mathbf{1B}^-$ and $\mathbf{2B}^-$, full crystallographic details, and complete author list for ref 27. This material is available free of charge via the Internet at http://pubs.acs.org.

■ AUTHOR INFORMATION

Corresponding Author

*Chisholm@chemistry.ohio-state.edu.

■ ACKNOWLEDGMENT

This material is based upon work supported by the National Science Foundation under Grant No. 0957191. We thank the National Science Foundation for financial support of this work, and P.B. acknowledges the Beckman Foundation for an undergraduate Beckman Scholarship.

■ REFERENCES

(1) Creutz, C.; Taube, H. *J. Am. Chem. Soc.* **1969**, *91*, 3988–3989.
(2) Lambert, C.; Nöll, G. *J. Am. Chem. Soc.* **1999**, *121*, 8434–8442.
(3) Nelsen, S. F.; Weaver, M. N.; Telo, J. P. *J. Am. Chem. Soc.* **2007**, *129*, 7036–7043.
(4) Robin, M. B.; Day, P. *Adv. Inorg. Chem. Radiochem.* **2010**, *10*, 247–403.
(5) D'Alessandro, D. M.; Keene, F. R. *Chem. Soc. Rev.* **2006**, *35*, 424–440.
(6) Badger, B.; Brocklehurst, B. *Trans. Faraday Soc.* **1970**, *66*, 2939.
(7) Marcus, R. A. *J. Chem. Phys.* **1956**, *24*, 966–978.
(8) Hush, N. S. *Prog. Inorg. Chem.* **1967**, *8*, 391–444.
(9) Sutin, N. *Prog. Inorg. Chem.* **1983**, *30*, 441–498.
(10) Brunschwig, B. S.; Creutz, C.; Sutin, N. *Chem. Soc. Rev.* **2002**, *31*, 168–184.
(11) Zhang, L. T.; Ko, J.; Ondrechen, M. J. *J. Am. Chem. Soc.* **1987**, *109*, 1666–1671.
(12) Chisholm, M. H. *Proc. Nat. Acad. Sci. U.S.A.* **2007**, *104*, 2563–70.
(13) Lear, B. J.; Chisholm, M. H. *Inorg. Chem.* **2009**, *48*, 10954–10971.
(14) Barybin, M. V.; Chisholm, M. H.; Dalal, N. S.; Holovics, T. H.; Patmore, N. J.; Robinson, R. E.; Zipse, D. J. *J. Am. Chem. Soc.* **2005**, *127*, 15182–15190.
(15) Barybin, M. V.; Chisholm, M. H.; Patmore, N. J.; Robinson, R. E.; Singh, N. *Chem. Commun.* **2007**, 3652–3654.
(16) Alberding, B. G.; Barybin, M. V.; Chisholm, M. H.; Gustafson, T. L.; Reed, C. R.; Robinson, R. E.; Patmore, N. J.; Singh, N.; Turro, C. *Dalton Trans.* **2010**, *39*, 1979–1984.
(17) Alberding, B. G.; Chisholm, M. H.; Chou, Y.; Ghosh, Y.; Gustafson, T. L.; Liu, Y.; Turro, C. *Inorg. Chem.* **2009**, *48*, 11187–11195.
(18) Chisholm, M. H.; Dann, A. S.; Dielmann, F.; Gallucci, J. C.; Patmore, N. J.; Ramnauth, R.; Scheer, M. *Inorg. Chem.* **2008**, *47*, 9248–9255.

(19) Cotton, F. A.; Murillo, C. A.; Walton, R. A. *Multiple Bonds between Metal Atoms*, 3rd ed.; Springer Science and Business Media, Inc.: New York, 2005; p 818.

(20) Szafert, S.; Gladysz, J. A. *Chem. Rev.* **2006**, *106*, 1–33.

(21) Dinolfo, P. H.; Coropceanu, V.; Brédas, J.; Hupp, J. T. *J. Am. Chem. Soc.* **2006**, *128*, 12592–12593.

(22) Dinolfo, P. H.; Hupp, J. T. *J. Am. Chem. Soc.* **2004**, *126*, 16814–16819.

(23) Dinolfo, P. H.; Williams, M. E.; Stern, C. L.; Hupp, J. T. *J. Am. Chem. Soc.* **2004**, *126*, 12989–13001.

(24) Telo, J. P.; Nelsen, S. F.; Zhao, Y. *J. Phys. Chem. A* **2009**, *113*, 7730–7736.

(25) Nelsen, S. F.; Konradsson, A. E.; Telo, J. P. *J. Am. Chem. Soc.* **2005**, *127*, 920–925.

(26) Cotton, F. A.; Daniels, L. M.; Hillard, E. A.; Murillo, C. A. *Inorg. Chem.* **2002**, *41*, 1639–1644.

(27) Frisch, M. J.; et al. *Gaussian 98*, revision A6; Gaussian Inc.: Pittsburgh, PA, 1998.

(28) Hehre, W. J.; Radom, L.; Schleyer, P. V.; Pople, J. A. *Ab initio Molecular Orbital Theory*; Wiley: New York, 1986.

(29) Lee, C.; Yang, W.; Parr, R. G. *Phys. Rev. B: Condens. Matter* **1988**, *37*, 785–789.

(30) Becke, A. D. *J. Chem. Phys.* **1993**, *98*, 5648–5652.

(31) Becke, A. D. *Phys. Rev A: Gen. Phys.* **1988**, *38*, 3098–3100.

(32) Andrae, D.; iuBermann, U.; H; Dolg, M.; Stoll, H.; PreuB, H. *Theor. Chim. Acta.* **1990**, *77*, 123–141.

(33) *GaussView*, version 3.09; Semichem Inc.: Shawnee Mission, KS, 2003.